Published in final edited form as:
Biomaterials. 2014 September ; 35(27): 7811–7818. doi:10.1016/j.biomaterials.2014.05.057.

Magnetization transfer contrast MRI for non-invasive assessment of innate and adaptive immune responses against alginate-encapsulated cells

Kannie W.Y. Chan[a,b,c,d], **Guanshu Liu**[a,b], **Peter C.M. van Zijl**[a,b], **Jeff W.M. Bulte**[a,b,d], and **Michael T. McMahon**[a,b,c,*]

[a]Russell H. Morgan Department of Radiology and Radiological Science, The Johns Hopkins University School of Medicine, Baltimore, MD 21287, USA

[b]F.M. Kirby Research Center for Functional Brain Imaging, Kennedy Krieger Institute, Baltimore, MD 21205, USA

[c]Center of Nanomedicine, The Johns Hopkins University School of Medicine, Baltimore, MD 21287, USA

[d]Cellular Imaging Section and Vascular Biology Program, Institute for Cell Engineering, Baltimore, MD 21205, USA

Abstract

By means of physical isolation of cells inside semi-permeable hydrogels, encapsulation has been widely used to immunoprotect transplanted cells. While spherical alginate microcapsules are now being used clinically, there still is little known about the patient's immune system response unless biopsies are obtained. We investigated the use of Magnetization Transfer (MT) imaging to non-invasively detect host immune responses against alginate capsules containing xenografted human hepatocytes in four groups of animals, including transplanted empty capsules (−Cells/−IS), capsules with live cells with (+LiveCells/+IS) and without immunosuppression (+LiveCells/−IS), and capsules with apoptotic cells in non-immunosuppressed animals (+DeadCells/−IS). The highest MT ratio (MTR) was found in +LiveCells/−IS, which increased from day 0 by 38% and 53% on days 7 and 14 after transplantation respectively, and corresponded to a distinctive increase in cell infiltration on histology. Furthermore, we show that macromolecular ratio maps based on MT data are more sensitive to cell infiltration and fibrosis than conventional MTR maps. Such maps showed a significant difference between +LiveCells/−IS (0.18±0.02) and +DeadCells/−IS (0.13±0.02) on day 7 ($P<0.01$) existed, which was not observed on MTR imaging. We conclude that MT imaging, which is clinically available, can be applied for non-invasive monitoring of the occurrence of a host immune response against encapsulated cells.

Corresponding author: mtmcmaho@gmail.com.

Keywords

Alginate microcapsules; cellular imaging; molecular imaging; immune response; MRI

1. Introduction

MRI has widely been used as a non-invasive tool to monitor cell transplantation in animals through iron oxide labeling of cells prior to transplantation [1–5]. This strategy has allowed (real-time) tracking of cell delivery and assessment of the initial tissue engraftment pattern. For certain types of transplantations, it is beneficial to employ hydrogels to immunoprotect cells after transplantation, in order to prolong cell survival. These hydrogels are formed from natural materials such as collagen, hyaluronic acid, chitosan, alginate, and gelatin [6–9], and can be designed to self-assemble [10] and include features which direct cell differentiation [8, 9, 11]. Alginate hydrogels have been shown to provide an immunological barrier for transplanted cells for long periods of time [12], and have undergone small scale trials in patients with several still ongoing [13], (NCT01736228; NCT01739829; NCT00790257; NCT00940173; NCT00981006). In recent work, an alternative strategy for cell imaging has been applied, labeling the hydrogels with contrast agents instead of directly labeling cells [14–16], which provides several benefits [17–25]. One benefit of this strategy is that the survival and function of the cells remains unaltered as they do not contain the label. Another is that smart contrast materials, such as pH-sensitive contrast agents, can allow monitoring the viability of encapsulated cells through detecting changes in pH [19].

One of the challenges of therapeutic cell transplantation is immunorejection of grafted cells. Inflammatory responses can occur in reaction to the alginate hydrogel [26–28], engrafted cells, the act of surgical transplantation, or combinations thereof [26]. Both the occurrence of a foreign body response (FBR) and a host-versus-graft immune response are considered to be major hurdles to successful transplantation [29]. These responses are complex and orchestrated, especially after implantation of cell grafts within biomaterials, and involve either an innate and/or an adaptive immune response [30]. These responses are characterized by an acute and a chronic phase. In the acute phase, inflammation, deposition of proteins and neutrophils [31], and activation of leukocytes take place. If inflammatory stimuli persist, there will be a chronic response involving macrophages and dendritic cells (Fig. 1). Alginate capsule implantation has been shown to induce a response by promoting macrophages and activating dendritic cells which then leads to the production of pro-inflammatory cytokines, and ultimately results in fibrosis [29, 31, 32]. In addition, crosstalk between infiltrating immune cells and the encapsulated cell graft can enhance fibrosis [33]. There are multiple adjustments which could be made to the transplantation protocol should there be a significant immune response. For example, auxiliary immunosuppression regimes can be administered to alleviate acute inflammation and halt progression to fibrosis, which may prolong cell survival time. Alternatively, improvements in the porosity, hydrophilicity, or surface properties of the hydrogel chosen to support the cell graft might minimize the FBR [6].

Hence, it is highly desirable to have non-invasive methods available that can monitor the occurrence and extent of an immune response early and serially over time, allowing

implementing modifications to existing protocols. In particular, an MRI method that can monitor cell infiltration or fibrosis and could be connected with the spatial location of the transplant would be crucial to improve therapeutic outcome. Magnetization transfer (MT) MR imaging, which generates contrast based on the concentration of semi-solid macromolecules and the rigidity of tissue [34–37], has the ability to probe the composition of tissue surrounding encapsulated cell grafts. By selectively saturating the semi-solid macromolecular proton pool in the region of the graft, a reduction in water signal can be produced with the amount of signal loss sensitive to the type of tissue and to changes in this tissue [38–40]. MT has been applied to monitor demyelination in multiple sclerosis [41], ischemia [42], and the extent of fibrosis in Crohn's disease [43]. Quantitative MT measurements have shown a decrease in the macromolecular fraction in apoptotic cells, indicating sensitivity to cellularity [44]. Changes in collagen concentration and other macromolecules can also be detected [45, 46]. To explore the applicability of MT imaging in monitoring graft rejection, we collected MT images for subcutaneously xenografted alginate capsules containing human HEPG2 hepatocytes in mice.

2. Materials and Methods

2.1. Preparation of diaCEST microcapsules

In brief, L-arginine containing liposomes were mixed with 2% alginate and cells, then electrosprayed into a 20 mM $BaCl_2$ bath to form beads. Beads were crosslinked with 0.1% protamine sulfate [14, 19, 20, 24] and then coated with the second layer of 0.15% alginate. L-arginine liposomes were prepared using the thin-film hydration method [47], and were typically ~150 nm in diameter. HepG2 hepatocytes were grown in Eagle's Minimum Essential Medium with 10% fetal bovine serum. Capsules containing dead HepG2 cells were prepared by treating HepG2 cells with 50 μM staurosporine prior to encapsulation. HepG2 cells were transduced to express luciferase using package lentivector (pLenti4-CMV-fLuc2) [17], to confirm cell survival vs. cell death using bioluminescent imaging (BLI).

2.2. Animal studies

All animal studies were performed in accordance with guidelines provided by our Institutional Animal Care and Use Committee. Balb/c mice (male, 6–8 weeks) were obtained from Jackson Laboratory. The animals were housed under standard pathogen-free conditions and had free access to water and standard laboratory chow. Encapsulated HepG2 hepatocytes were transplanted subcutaneously (2,000–3,000 capsules containing a total of ~0.5 million cells) into the lower abdomen of Balb/c mice (20–25 g). MRI and histological studies were performed on four groups of animals: 1) immunosuppressed mice transplanted with microcapsules containing live hepatocytes (+LiveCells/+IS, n=3); 2) mice without immunosuppression transplanted with microcapsules containing live hepatocytes (+LiveCells/−IS, n=3), 3) microcapsules containing dead hepatocytes (+DeadCells/−IS, n=3) and 4) microcapsules without cells (−Cells/−IS, n=3). Cell containing alginate microcapsules (diaCEST capsules) were prepared as reported previously [19]. For surgery, mice were kept under 1–2% isoflurane anesthesia with encapsulated HepG2 cells transplanted subcutaneously into the lower abdomen of mice for the +LiveCells/+IS, +LiveCells/−IS, +DeadCells/−IS and −Cells/−IS groups. Mice in the +Cells/+IS group

received a daily administration of both rapamycin and FK-506 at 1 mg/kg intraperitoneal (i.p.).

2.3. Imaging Protocol

Mice were anesthetized using isofluorane and positioned in a 9.4T horizontal bore Bruker Biospec scanner. MT, T_1 and T_2 images were collected for four groups of mice: +LiveCells/+IS (n=3), +LiveCells/−IS (n=3), +DeadCells/−IS (n=3) and −Cells/−IS (n=3). MT images were acquired on day 0, 1, 7, 14, and 28 post-transplantation with saturation offsets of −50, −25, −12.5, −5, and −2.5 ppm using a continuous-wave (CW) saturation pulse of (B_1=3.6 μT, 3 sec). The imaging parameters were repetition time (TR)=5 sec, RARE factor=10, effective echo time (TE)=5 msec. R_2 relaxation data were acquired using a multi-slice multi-echo sequence with 16 echoes, TE=10, 20, 30, 40, 50, 60, 70, 80, 90, 100, 110, 120, 130, 140, 150, and 160 ms. R_1 relaxation data were acquired using a saturation recovery method with the RARE imaging sequence, TR=0.2, 0.5, 1, 2, 3, 5, 7.5, and 10 sec.

Images were processed using custom-written Matlab scripts with $MTR=(S_0-S_{SAT}(\omega))/S_0$ where S_0 and $S_{SAT}(\omega)$ are the signal amplitude measured without and with a saturation pulse at frequency ω, respectively [48]. The ratio of parameters characterizing the amount of water magnetization lost through exchange with macromolecular protons to the recovery of magnetization through longitudinal relaxation was calculated using $R*f_{0B}/R_{1A}$, where R is the macromolecular exchange rate, f_{0B} is the proton fraction of the macromolecular pool, and R_{1A} is the longitudinal relaxation of the free water pool [44]. R_{1A} and R_{2A} were independently obtained from $R*f_{0B}$ through standard exponential fits to the acquired R_1 and R_2 data, respectively.

2.4. Histology

Samples of excised subcutaneously microcapsule regions were fixed in buffered formalin, embedded in paraffin, and sectioned. Specimens were stained with hematoxylin and eosin (H&E) and Masson trichrome. ImageJ was used to measure the number of nuclei in the H&E stained sections. For Masson trichrome stain, the nucleus is black, cytoplasm and erythrocytes are red, and collagen fibers are blue.

Statistical analyses were performed using a two-way ANOVA test for comparison of MTR and $R*f_{0B}/R_{1A}$ among the groups and times, and a one-way ANOVA test for comparison between the groups. Spearman correlation was performed between the macromolecular ratio and number of nuclei measured from histology.

3. Results

3.1. MT imaging

The source of magnetization transfer contrast is transfer of signal loss between macromolecular and water protons [49, 50]. The extent of transfer depends on the relaxation times of the protons, the relative population sizes, and the MT exchange rate. Since there are a number of macromolecules implicated in immune reactions, we investigated how MT

images change after implantation of alginate capsules into mice (Fig. 1). Figure 2 displays representative MTR maps at −12.5 ppm after subcutaneous transplantation of alginate capsules in four groups of mice: alginate capsules without cells (−Cells/−IS), capsules containing live hepatocytes transplanted into mice receiving immunosuppression (+LiveCells/+IS), transplanted alginate capsules containing live hepatocytes without immunosuppressants (+LiveCells/−IS), and alginate capsules containing dead hepatocytes without immunosuppression (+DeadCells/−IS). The MTR values for ROIs drawn over the region containing alginate capsules were not significantly different among the four groups on day 0, with an average MTR of 0.27±0.05. Comparing the images on days 7 and 14 revealed that the average MTR values were significantly higher in the cell-containing groups that did not receive immunosuppression (i.e. +LiveCells/−IS and +DeadCells/−IS in Fig. 2). This effect was particularly pronounced on day 14 with an average MTR value of 0.45 for the +LiveCells/−IS group, which was 53% higher than on day 0, and even higher (17% higher than day 0) at 28 days. The average MTR value of 0.42 for the +DeadCells/−IS group on day 14 was also significantly higher than that of +LiveCells/+IS ($P<0.001$). MTR maps did not display a significant difference between the +LiveCells/−IS and +DeadCells/−IS (Fig. 2B). Furthermore, there was no significant change in MTR in both the +LiveCells/+IS and −Cells/−IS groups (n=3; Fig. 2). These results indicate that the changes in MTR signal are primarily caused by an (adaptive) immune response against the cell graft in the absence of immunosuppression, regardless whether the cells are dead or alive. The innate immune response (foreign body reaction to the alginate capsule in the absence of cells) appears to play a relatively minor role.

3.2. Using MT to determine macromolecular ratios for animals containing live vs. dead hepatocytes

In order to better understand our MT imaging data and better separate the two cell-containing groups of mice not treated with immunosuppressants, we fitted the images as a function of saturation frequency on a pixel-by-pixel basis according to a two-pool model. The fits resulted in maps of the macromolecular fraction f_{0B} and the ratio: R^*f_{0B}/R_{1A}. As shown in Figure 3, we observed significant differences between the groups (Fig. 3, n=3), with the macromolecular ratios for the capsule region in the +LiveCells/−IS group significantly higher than in the +DeadCells/−IS group (n=3, $P<0.01$; Fig. 3C) on days 7, 14, and 28 post-transplantation. This is not observed in the MTR (Fig. 2B). This implies that more semi-solid protons are present in the capsule region presumably because the HepG2 cells within the alginate actively produce soluble xenogeneic molecules (small proteins and cytokines), that diffuse out of the capsules and attract immune cells. The number of immune cells infiltrating into the capsules region is expected to be lower when dead hepatocytes are encapsulated in alginate, as they cannot actively release cytokines. The macromolecular ratio dropped on day 28 but the difference between these two groups was still significant (n=3, $P<0.01$). This is likely caused by the release of xenogeneic protein and other macromolecule (fragments), which are released upon cell death. To examine the sensitivity of the macromolecular ratios for detecting cell infiltration, we compared the maps on day 1 among the three cell-containing groups (Fig. 6). There was a higher R^*f_{0B}/R_{1A} and f_{0B} in groups without immunosuppression, indicating a higher macromolecular content for these animals. In contrast, both R^*f_{0B}/R_{1A} and f_{0B} showed no changes over 28 days in the −Cells/

−IS group (Fig. 6). The overall macromolecular ratio maps thus correspond to the MTR maps, but have higher sensitivity for detecting differences between the four groups.

3.3. Histological analysis

In order to determine whether or not there were visible histological changes in the tissue that corresponded to the differences that we observed with our MTR and macromolecular ratio maps, we performed H&E and Masson trichrome stains on excised tissues. First, we looked at the relative amount of host cells infiltrating into the capsule regions among the groups of animals on days 7, 14, and 28 post-transplantation. The number of cells surrounding the capsules was highest in the +LiveCells/−IS group, followed by the +DeadCells/−IS group and the lowest for the +LiveCells/+IS and −Cells/−IS group (Fig. 4A, green arrows). The day 14 staining displayed a particularly large number of infiltrating cells in the +LiveCells/−IS and +DeadCells/−IS groups (Fig. 4B), which is in agreement with the high MTR and macromolecular ratios in the capsule regions for the maps in Figs. 2 and 3. For the +LiveCells/−IS animals, the number of cells infiltrating into the capsule region was pronounced on day 7. Moreover, the cell-containing groups with the lowest MTR and macromolecular ratio (+LiveCells/+IS) had the lowest number of infiltrating cells (Fig. 4), as a result the of the stringent rapamycin/FK506 immunosuppression regimen that was used. The H&E stainings of the −Cells/−IS group was comparable to that of +LiveCells/+IS group with a low number of infiltrating cells over 14 days (Fig. 4). Blood cells were observed in both non-immunosuppressed cell groups on day 14, which has been described previously [33] (Fig. 4, yellow arrows). The number of nuclei measured in H&E sections correlated with the macromolecular ratio ($r=0.96$ and $P<0.0001$, Fig. 4C).

3.4. Comparing the periphery and center of transplanted capsule regions

The macromolecular maps in the capsule region showed some heterogeneity which we decided to investigate further. In particular, we found that the macromolecular ratio maps for the +LiveCells/−IS mice showed a different pattern than for the +DeadCells/−IS mice (Fig. 5). The pixels in the capsule regions of the +LiveCells/−IS group had high values at the center of the capsule region and low values in the periphery, while the +DeadCells/−IS group had high values throughout the capsule region. After performing ROI analysis, interestingly the +LiveCells/−IS animals had significantly higher macromolecular ratios in the center as compared to the periphery (Fig. 5B) on day 7 ($n=3$; *, $P<0.05$) and on day 14 ($n=3$; **, $P<0.005$), which was not observed in the +DeadCells/−IS animals (Fig. 5C). Partial volume effects could influence the pixels in the periphery. To minimize this, 1-mm slices in the middle of the transplanted capsule region were chosen and checked with the adjacent slices. In addition, differences were observed between the center and the periphery in the +LiveCells/−IS group (e.g. +LiveCells/−IS, D14 in Fig. 3), but not in the other groups. We then examined the H&E sections of the animals in these groups and found differences in the morphology at the center (Fig. 5D). In particular, the center of the capsule regions for the +LiveCells/−IS group displayed more granular structures while the periphery showed layers of infiltrating cells around the capsules (Fig. 5D, yellow arrows). For the +DeadCells/−IS group, the center and the periphery showed a similar density of infiltrating cells, without granulation at the center of the capsule region (Fig. 5E, yellow arrows). With these observations, we further examined the tissues by performing Masson trichrome stains

to detect the presence of macromolecules that are present during the chronic phase of FBR, characterized by fibrosis and collagen formation. In this stain, collagen is blue, nuclei are black and muscle, cytoplasm and keratin are red. As compared the periphery and the center of the +LiveCells/−IS capsule region on day 14 post-transplantation, a larger amount of collagen fibers (blue) were found at the center of the region for the +LiveCells/−IS group (Fig. 5E, yellow arrows) than within the periphery. Negligible collagen staining was observed in the +DeadCells/−IS group (Fig. 5F).

Discussion

The current study shows that MT imaging can be used to detect changes in tissue after transplantation of encapsulated cells. In order to investigate the variations which we might detect based on the complexity of the host immune response to alginate-encapsulated cell grafts, we studied immunocompetent mice with and without use of immunosuppressants. The −Cells/−IS group was used as a control for the innate immune response, showing that surface of the alginate capsule itself elicited a minimal FBR, while the +LiveCells/−IS and +Deadcells/−IS groups were studied to investigate the immune responses with highly immunogenic and mildly immunogenic cells, respectively. The +LiveCells/−IS and +DeadCells/−IS groups were valuable to examine if MT imaging could be used to determine whether there were differences in immune responses between shedded xenogeneic molecules between live and dead cells. The MTR values were comparable among the four groups on day 0, but increased in animals without immunosuppression on day 7 and day 14. A large number of infiltrating cells is expected for the +LiveCells/−IS animals because of the presence of highly immunogenic (xenogeneic) human hepatocytes in the alginate capsule, which was confirmed by the H&E stains. The apoptotic cells in +DeadCells/−IS elicited a somewhat milder cell infiltration (Fig. 4, green arrows). As the capsules prevent direct cell-cell contact, the cell infiltration must be caused either by soluble xenogeneic molecules that exit the semi-permeable capsules in addition to the capsule surface/FBR [51]. From previous studies it is known that the capsules allow molecules that are smaller than 75 kDa [14, 19] to pass through. Since dead cells are incapable of producing soluble molecules and cytokines continuously, the increase in MTR was less substantial than that for +LiveCells/−IS group.

Immune responses in the presence of both foreign body material on the capsule surface and cellular antigens are orchestral and complex; in general the changes in MTR from day 7 onwards correspond to a chronic phase, leading to fibrosis (Fig. 1). The histological data we collected as part of this study showed that the increase in MTR values and macromolecular ratios are associated with the extent of infiltrating cells in the capsule region. These immune cells consist of macrophages, neutrophils or dendritic cells [52]. Although MRI currently is not able to identify these cells, a distinctive difference was observed in both MTR and macromolecular ratio between the immunosuppressed group and the non-immunosuppressed groups (Fig. 2). Capsules in both the +LiveCells/−IS and +DeadCells/−IS were surrounded by a large number of cells on day 14 post-transplantation, including red blood cells indicating neovascularization (Fig. 4, yellow arrows). The residual dying cells in the +DeadCells/−IS can still elicit responses that recruit inflammatory cells [33], therefore, there was a subtle difference in both the MTR and the number of infiltrated cells between the

+LiveCells/−IS and +DeadCells/−IS. Both groups exhibited neovascularization on day 14, which is likely induced by low oxygen conditions with a high cell density at the subcutaneous transplanted capsule regions.

To further identify the subtle differences in immune responses in the +LiveCells/−IS and +DeadCells/−IS, we quantified the MT properties of the capsule region through fitting the saturation frequency dependent saturation images to a two-pool model, since MT contrast depends on the relaxation times and line shape of water signal [53]. The macromolecular ratio and maps provide an assessment of the macromolecular content of tissues and spatial changes, and showed a significant difference between the +LiveCells/−IS and +DeadCells/−IS groups ($n=3$, $P<0.01$). The morphological features of the +LiveCells/−IS group were also different in the central area of infiltrating cells of the capsule region than at the peripherial according to the H&E stains (Fig. 5D). In the center of the capsule region, areas surrounding the capsules were granular with a lower density of cells. Masson trichrome staining showed that the granular structures in H&E were collagen fibers (Fig. 5F, yellow arrows). The center of the +LiveCells/−IS capsule region was mainly composed of collagen and erythrocytes, and since the center is expected to be the least perfused and the encapsulated cells lack of vasculaturization and oxygen, the center has a reduced cellularity. Similarly, the center of the +DeadCells/−IS, was not as well perfused as the periphery, however, there were no living HepG2 cells in the capsules actively producing xenogeneic molecules to recruit immune cells and sustain the response. These observations might explain our result of no difference between the center and the periphery (Fig. 5E), and the absence of collagen fibers (Fig. 5G).

Transient immunosuppression regimes are preferred for suppressing acute inflammation. If alginate capsules can protect the grafts from direct interacting with immune cells, the grafts should be able to survive longer *in vivo*. Since the macromolecular ratios provides a number which relates to the macromolecular content of tissues, including the number of infiltrating cells, the amount of collagen, and amount of fibrosis, obtaining macromolecular ratio maps might allow more timely application and modification of immunosuppressant regimes to improve therapeutic outcomes. During the acute phase, which is day 1 post-transplantation, the macromolecular ratios and f_{0B} were slightly higher in both the +LiveCells/−IS and +DeadCells/−IS groups than that in the +LiveCells/+IS group and the +LiveCells/−IS. f_{0B} was slightly higher than +DeadCells/−IS (Fig. 6), although the changes in f_{0B} on day 1 were not significant. The observed trend indicates that measuring these macromolecular ratios allows one to assess the amount of cell infiltration following transplantation. Unlike biopsies and other methods for assessing immune responses or FBR in cell therapies, MRI is non-invasive and provides a good spatial resolution and regional information around the transplanted capsules. We anticipate our MT/macromolecular ratio imaging approach to be generally applicable in other scenarios where a host immune response against implanted biomaterials may be present, including but not limited to hyaluronic acid hydrogels [54].

5. Conclusions

We have shown the potential of using conventional MT imaging and quantitative macromolecular ratio maps to monitor the extent of the innate and adaptive immune

responses in encapsulated cell therapy. Extensive cell infiltration and fibrosis can be non-invasively detected with MT imaging with good spatial resolution. Moreover, the macromolecular ratio maps display heterogeneity, which corresponds to differences in collagen content between the center and the periphery of the surrounding cells. The use of MT imaging may enable timely adjustments to immunosuppressive drug regimens in future clinical use.

Acknowledgments

The authors sincerely thank the NIH for support through: R01EB012590, R01EB015031, R01EB015032, RO1EB007825, and MSCRFII-0161-00.

References

1. Bulte JW, Kraitchman DL. Iron oxide MR contrast agents for molecular and cellular imaging. NMR Biomed. 2004; 17:484–99. [PubMed: 15526347]
2. Heyn C, Ronald JA, Ramadan SS, Snir JA, Barry AM, MacKenzie LT, et al. In vivo MRI of cancer cell fate at the single-cell level in a mouse model of breast cancer metastasis to the brain. Magn Reson Med. 2006; 56:1001–10. [PubMed: 17029229]
3. Shapiro EM, Skrtic S, Sharer K, Hill JM, Dunbar CE, Koretsky AP. MRI detection of single particles for cellular imaging. Proc Natl Acad Sci U S A. 2004; 101:10901–6. [PubMed: 15256592]
4. Medarova Z, Moore A. MRI as a tool to monitor islet transplantation. Nat Rev Endocrinol. 2009; 5:444–52. [PubMed: 19546863]
5. Arbab AS, Bashaw LA, Miller BR, Jordan EK, Bulte JW, Frank JA. Intracytoplasmic tagging of cells with ferumoxides and transfection agent for cellular magnetic resonance imaging after cell transplantation: methods and techniques. Transplantation. 2003; 76:1123–30. [PubMed: 14557764]
6. Seliktar D. Designing cell-compatible hydrogels for biomedical applications. Science. 2012; 336:1124–8. [PubMed: 22654050]
7. Chang CY, Chan AT, Armstrong PA, Luo HC, Higuchi T, Strehin IA, et al. Hyaluronic acid-human blood hydrogels for stem cell transplantation. Biomaterials. 2012; 33:8026–33. [PubMed: 22898181]
8. Sharma B, Fermanian S, Gibson M, Unterman S, Herzka DA, Cascio B, et al. Human cartilage repair with a photoreactive adhesive-hydrogel composite. Sci Transl Med. 2013; 5:167ra6.
9. DeVolder R, Kong HJ. Hydrogels for in vivo-like three-dimensional cellular studies. Wiley Interdiscip Rev Syst Biol Med. 2012; 4:351–65. [PubMed: 22615143]
10. Kopecek J, Yang J. Smart self-assembled hybrid hydrogel biomaterials. Angew Chem Int Ed Engl. 2012; 51:7396–417. [PubMed: 22806947]
11. DeForest CA, Anseth KS. Advances in bioactive hydrogels to probe and direct cell fate. Annu Rev Chem Biomol Eng. 2012; 3:421–44. [PubMed: 22524507]
12. Nilsson B, Korsgren O, Lambris JD, Ekdahl KN. Can cells and biomaterials in therapeutic medicine be shielded from innate immune recognition? Trends Immunol. 2010; 31:32–8. [PubMed: 19836998]
13. Elliott RB, Escobar L, Tan PL, Muzina M, Zwain S, Buchanan C. Live encapsulated porcine islets from a type 1 diabetic patient 9.5 yr after xenotransplantation. Xenotransplantation. 2007; 14:157–61. [PubMed: 17381690]
14. Barnett BP, Arepally A, Karmarkar PV, Qian D, Gilson WD, Walczak P, et al. Magnetic resonance-guided, real-time targeted delivery and imaging of magnetocapsules immunoprotecting pancreatic islet cells. Nat Med. 2007; 13:986–91. [PubMed: 17660829]
15. Shen F, Li AA, Gong YK, Somers S, Potter MA, Winnik FM, et al. Encapsulation of recombinant cells with a novel magnetized alginate for magnetic resonance imaging. Hum Gene Ther. 2005; 16:971–84. [PubMed: 16076255]

16. Noth U, Grohn P, Jork A, Zimmermann U, Haase A, Lutz J. 19F-MRI in vivo determination of the partial oxygen pressure in perfluorocarbon-loaded alginate capsules implanted into the peritoneal cavity and different tissues. Magn Reson Med. 1999; 42:1039–47. [PubMed: 10571925]
17. Link TW, Arifin DR, Long CM, Walczak P, Muja N, Arepally A, et al. Use of magnetocapsules for in vivo visualization and enhanced survival of xenogeneic HepG2 Cell Transplants. Cell Med. 2012; 4:77–84. [PubMed: 23293747]
18. Kim J, Arifin DR, Muja N, Kim T, Gilad AA, Kim H, et al. Multifunctional capsule-in-capsules for immunoprotection and trimodal imaging. Angew Chem Int Ed Engl. 2011; 50:2317–21. [PubMed: 21351344]
19. Chan KW, Liu G, Song X, Kim H, Yu T, Arifin DR, et al. MRI-detectable pH nanosensors incorporated into hydrogels for in vivo sensing of transplanted-cell viability. Nature Materials. 2013; 12:268–75.
20. Barnett BP, Arepally A, Stuber M, Arifin DR, Kraitchman DL, Bulte JW. Synthesis of magnetic resonance-, X-ray- and ultrasound-visible alginate microcapsules for immunoisolation and noninvasive imaging of cellular therapeutics. Nature protocols. 2011; 6:1142–51.
21. Barnett BP, Ruiz-Cabello J, Hota P, Liddell R, Walczak P, Howland V, et al. Fluorocapsules for improved function, immunoprotection, and visualization of cellular therapeutics with MR, US, and CT imaging. Radiology. 2011; 258:182–91. [PubMed: 20971778]
22. Barnett BP, Kraitchman DL, Lauzon C, Magee CA, Walczak P, Gilson WD, et al. Radiopaque alginate microcapsules for X-ray visualization and immunoprotection of cellular therapeutics. Molecular pharmaceutics. 2006; 3:531–8. [PubMed: 17009852]
23. Arifin DR, Manek S, Call E, Arepally A, Bulte JW. Microcapsules with intrinsic barium radiopacity for immunoprotection and X-ray/CT imaging of pancreatic islet cells. Biomaterials. 2012; 33:4681–9. [PubMed: 22444642]
24. Arifin DR, Long CM, Gilad AA, Alric C, Roux S, Tillement O, et al. Trimodal gadolinium-gold microcapsules containing pancreatic islet cells restore normoglycemia in diabetic mice and can be tracked by using US, CT, and positive-contrast MR imaging. Radiology. 2011; 260:790–8. [PubMed: 21734156]
25. Arifin DR, Kedziorek DA, Fu Y, Chan KW, McMahon MT, Weiss CR, et al. Microencapsulated cell tracking. NMR Biomed. 2013; 26:850–9. [PubMed: 23225358]
26. Hernandez RM, Orive G, Murua A, Pedraz JL. Microcapsules and microcarriers for in situ cell delivery. Adv Drug Deliv Rev. 2010; 62:711–30. [PubMed: 20153388]
27. Espevik T, Otterlei M, Skjak-Braek G, Ryan L, Wright SD, Sundan A. The involvement of CD14 in stimulation of cytokine production by uronic acid polymers. Eur J Immunol. 1993; 23:255–61. [PubMed: 7678226]
28. Otterlei M, Ostgaard K, Skjak-Braek G, Smidsrod O, Soon-Shiong P, Espevik T. Induction of cytokine production from human monocytes stimulated with alginate. J Immunother (1991). 1991; 10:286–91. [PubMed: 1931864]
29. Franz S, Rammelt S, Scharnweber D, Simon JC. Immune responses to implants - a review of the implications for the design of immunomodulatory biomaterials. Biomaterials. 2011; 32:6692–709. [PubMed: 21715002]
30. Morais JM, Papadimitrakopoulos F, Burgess DJ. Biomaterials/tissue interactions: possible solutions to overcome foreign body response. AAPS J. 2010; 12:188–96. [PubMed: 20143194]
31. Jones KS. Effects of biomaterial-induced inflammation on fibrosis and rejection. Semin Immunol. 2008; 20:130–6. [PubMed: 18191409]
32. Babensee JE. Interaction of dendritic cells with biomaterials. Semin Immunol. 2008; 20:101–8. [PubMed: 18054498]
33. Swartzlander MD, Lynn AD, Blakney AK, Kyriakides TR, Bryant SJ. Understanding the host response to cell-laden poly(ethylene glycol)-based hydrogels. Biomaterials. 2013; 34:952–64. [PubMed: 23149012]
34. Wolff SD, Balaban RS. Magnetization transfer contrast (MTC) and tissue water proton relaxation in vivo. Magn Reson Med. 1989; 10:135–44. [PubMed: 2547135]
35. Wolff SD, Balaban RS. Magnetization transfer imaging: practical aspects and clinical applications. Radiology. 1994; 192:593–9. [PubMed: 8058919]

36. Bouvignies G, Kay LE. Measurement of proton chemical shifts in invisible states of slowly exchanging protein systems by chemical exchange saturation transfer. J Phys Chem B. 2012; 116:14311–7. [PubMed: 23194058]
37. Anderson JM, Rodriguez A, Chang DT. Foreign body reaction to biomaterials. Semin Immunol. 2008; 20:86–100. [PubMed: 18162407]
38. Balaban RS, Ceckler TL. Magnetization transfer contrast in magnetic resonance imaging. Magn Reson Q. 1992; 8:116–37. [PubMed: 1622774]
39. Henkelman RM, Huang X, Xiang QS, Stanisz GJ, Swanson SD, Bronskill MJ. Quantitative interpretation of magnetization transfer. Magn Reson Med. 1993; 29:759–66. [PubMed: 8350718]
40. Morrison C, Henkelman RM. A model for magnetization transfer in tissues. Magn Reson Med. 1995; 33:475–82. [PubMed: 7776877]
41. Dousset V, Grossman RI, Ramer KN, Schnall MD, Young LH, Gonzalez-Scarano F, et al. Experimental allergic encephalomyelitis and multiple sclerosis: lesion characterization with magnetization transfer imaging. Radiology. 1992; 182:483–91. [PubMed: 1732968]
42. Makela Hi Fau-Kettunen MI, Kettunen Mi Fau-Grohn OHJ, Grohn Oh Fau-Kauppinen RA, Kauppinen RA. Quantitative T(1rho) and magnetization transfer magnetic resonance imaging of acute cerebral ischemia in the rat. J Cereb Blood Flow Metab. 2002; 22:547–58. [PubMed: 11973427]
43. Adler J, Swanson SD, Schmiedlin-Ren P, Higgins PD, Golembeski CP, Polydorides AD, et al. Magnetization transfer helps detect intestinal fibrosis in an animal model of Crohn disease. Radiology. 2011; 259:127–35. [PubMed: 21324841]
44. Bailey C, Desmond KL, Czarnota GJ, Stanisz GJ. Quantitative magnetization transfer studies of apoptotic cell death. Magnetic resonance in medicine. 2011; 66:264–9. [PubMed: 21695728]
45. Harel A, Eliav U, Akselrod S, Navon G. Magnetization transfer based contrast for imaging denatured collagen. J Magn Reson Imaging. 2008; 27:1155–63. [PubMed: 18425836]
46. Wang C, Witschey W, Goldberg A, Elliott M, Borthakur A, Reddy R. Magnetization transfer ratio mapping of intervertebral disc degeneration. Magn Reson Med. 2010; 64:1520–8. [PubMed: 20677229]
47. Zhao JM, Har-el YE, McMahon MT, Zhou J, Sherry AD, Sgouros G, et al. Size-induced enhancement of chemical exchange saturation transfer (CEST) contrast in liposomes. J Am Chem Soc. 2008; 130:5178–84. [PubMed: 18361490]
48. Stanisz GJ, Webb S, Munro CA, Pun T, Midha R. MR properties of excised neural tissue following experimentally induced inflammation. Magn Reson Med. 2004; 51:473–9. [PubMed: 15004787]
49. Henkelman RM, Stanisz GJ, Graham SJ. Magnetization transfer in MRI: a review. NMR Biomed. 2001; 14:57–64. [PubMed: 11320533]
50. Gareau PJ, Rutt BK, Karlik SJ, Mitchell JR. Magnetization transfer and multicomponent T2 relaxation measurements with histopathologic correlation in an experimental model of MS. J Magn Reson Imaging. 2000; 11:586–95. [PubMed: 10862056]
51. Strand BL, Ryan TL, In't Veld P, Kulseng B, Rokstad AM, Skjak-Brek G, et al. Poly-L-Lysine induces fibrosis on alginate microcapsules via the induction of cytokines. Cell Transplant. 2001; 10:263–75. [PubMed: 11437072]
52. Reid B, Gibson M, Singh A, Taube J, Furlong C, Murcia M, et al. PEG hydrogel degradation and the role of the surrounding tissue environment. J Tissue Eng Regen Med. 201310.1002/term.1688
53. Branco MC, Pochan DJ, Wagner NJ, Schneider JP. Macromolecular diffusion and release from self-assembled beta-hairpin peptide hydrogels. Biomaterials. 2009; 30:1339–47. [PubMed: 19100615]
54. Liang Y, Walczak P, Bulte JW. The survival of engrafted neural stem cells within hyaluronic acid hydrogels. Biomaterials. 2013; 34:5521–9. [PubMed: 23623429]

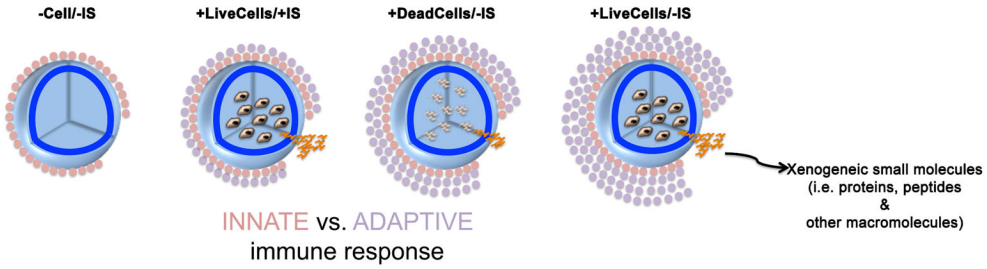

Fig. 1.

Cartoon depicting a schematic representation of the host immune response following transplantation of encapsulated cells in the four groups of mice: −Cells/−IS, +LiveCells/+IS, +DeadCells/−IS and +LiveCells/−IS.

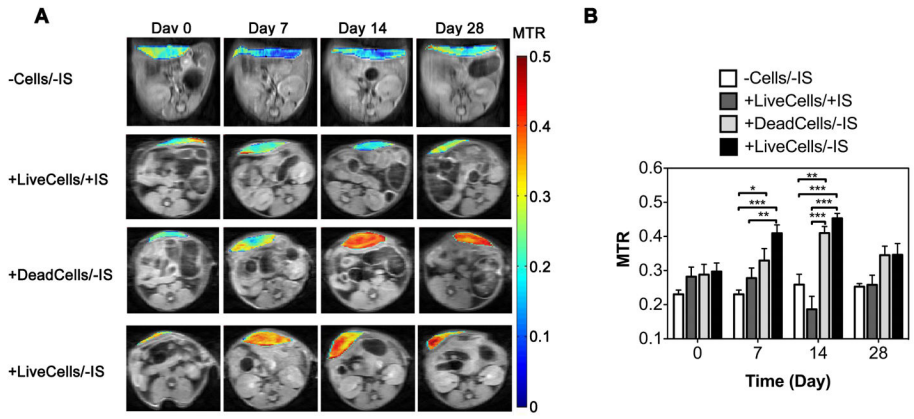

Fig. 2.

(A) Magnetization transfer ratio (MTR) maps at −12.5 ppm of representative mice with and without encapsulated hepatocytes in the −Cells/−IS, +LiveCells/+IS, +DeadCells/−IS, and +LiveCells/−IS groups at 0, 7, 14, and 28 days post-transplantation. (B) MTR (n=3) for ROIs drawn over the implanted capsule region in the four groups at the corresponding time points (*, P<0.05; **, P<0.01; ***, P< 0.001), indicating significant differences between the +IS and −IS group.

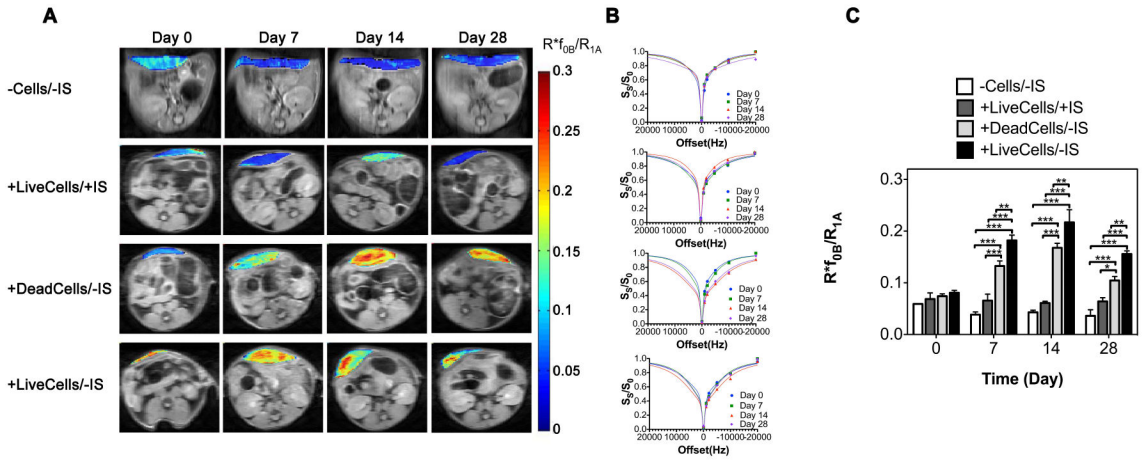

Fig. 3.

(A) Macromolecular ratio (R^*f_{0B}/R_{1A}) maps at −12.5 ppm for mice of representative mice with and without encapsulated hepatocytes in the −Cells/−IS, +LiveCells/+IS, +DeadCells/−IS, and + LiveCells/−IS groups at 0, 7, 14, and 28 days post-transplantation. (B) Fits of the frequency dependent MT data for the corresponding mice in A. (C) Macromolecular ratio data for days 0,7, 14, and 28 in the four groups (n=3; *, P<0.05; **, P<0.01; ***, P<0.001). A significant difference was found between the +LiveCells/−IS and +DeadCells/−IS group, which was not observed in the MTR shown in Fig. 2.

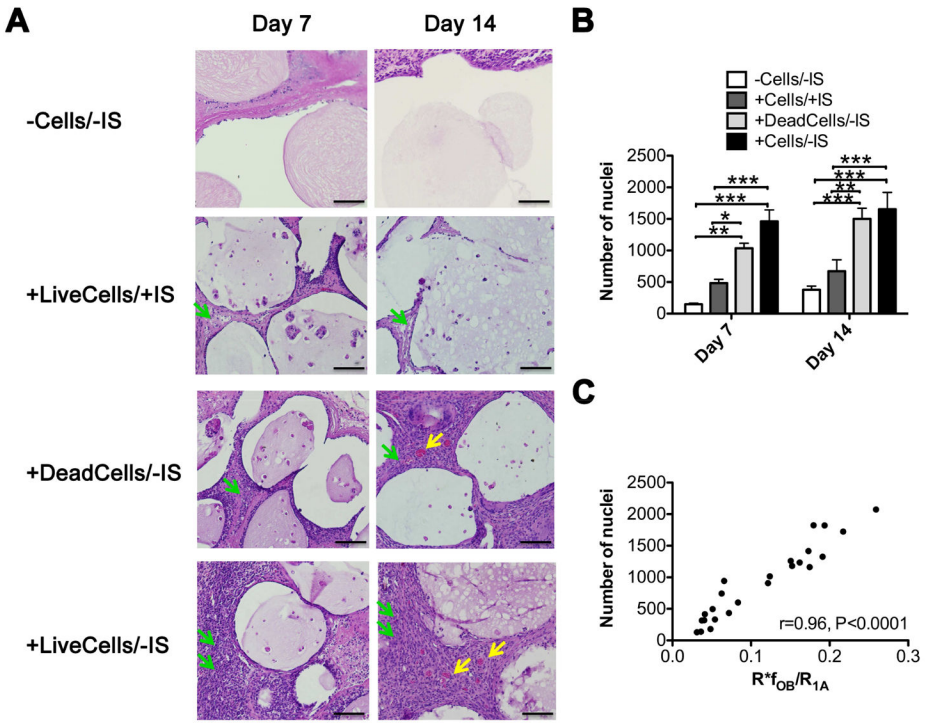

Fig. 4.

(A) Hematoxylin and eosin (H&E) staining of subcutaneous capsule regions for representative −Cells/−IS, +LiveCells/+IS, +DeadCells/−IS and +LiveCells/−IS mice on day 7 and day 14 post-transplantation, with regions having infiltrating cells (green arrows) and neovascularization (yellow arrows). (Scale bar = 50 μm). (B) The number of nuclei measured in H&E sections was significantly higher in +LiveCells/−IS and +DeadCells/−IS group than that in −Cells/−IS and +LiveCells/+IS groups (*, P<0.05; **, P<0.01; ***, P<0.001), and (C) its correlation with the macromolecular ratio (R^*f_{0B}/R_{1A}) was significant with r=0.96 and P<0.0001.

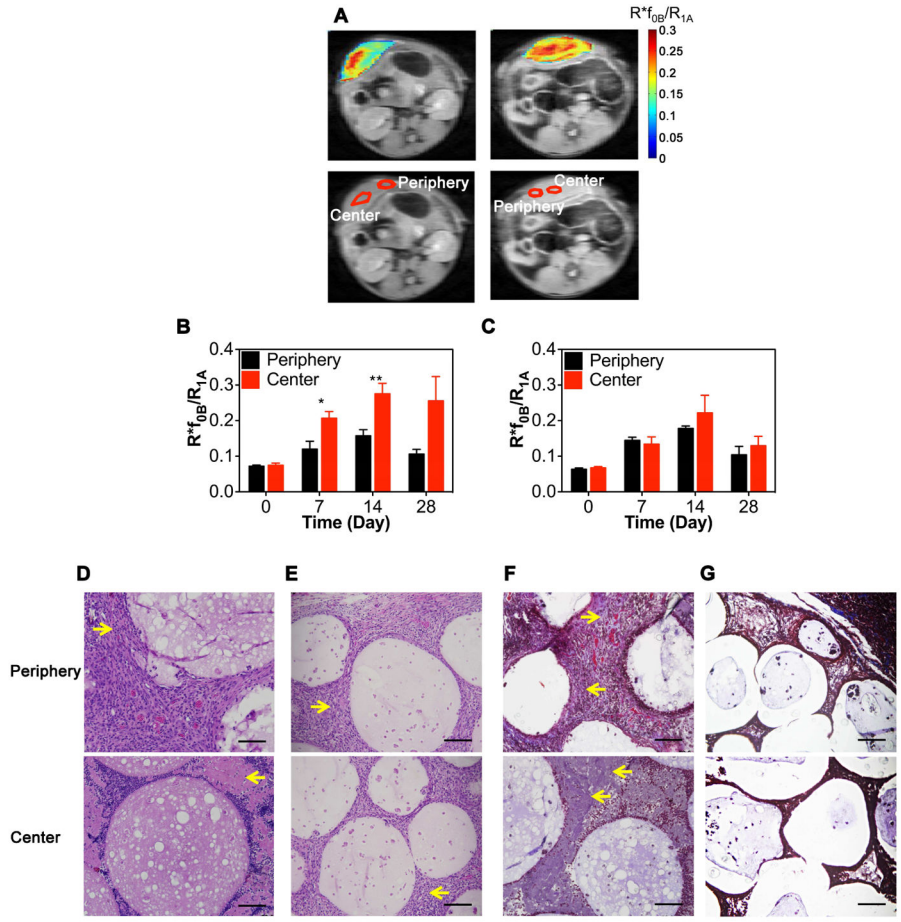

Fig. 5.

(A) Macromolecular ratio maps and ROIs for the center and periphery of the transplanted capsule regions of representative mice in the +LiveCells/−IS (right) and +DeadCells/−IS (left) groups. (B) Corresponding ratios for +LiveCells/−IS group (n=3), and (C) for +DeadCells/−IS group (n=3), (*, P<0.05; **, P<0.01). (D) H&E staining showing the periphery and center for a representative mouse in the +LiveCells/−IS group and (E) in the +DeadCells/−IS group; Masson trichrome stains with collagen in blue for the periphery and center for: (F) the +LiveCells/−IS group and (G) the +DeadCells/−IS group. (Scale bar = 50 μm).

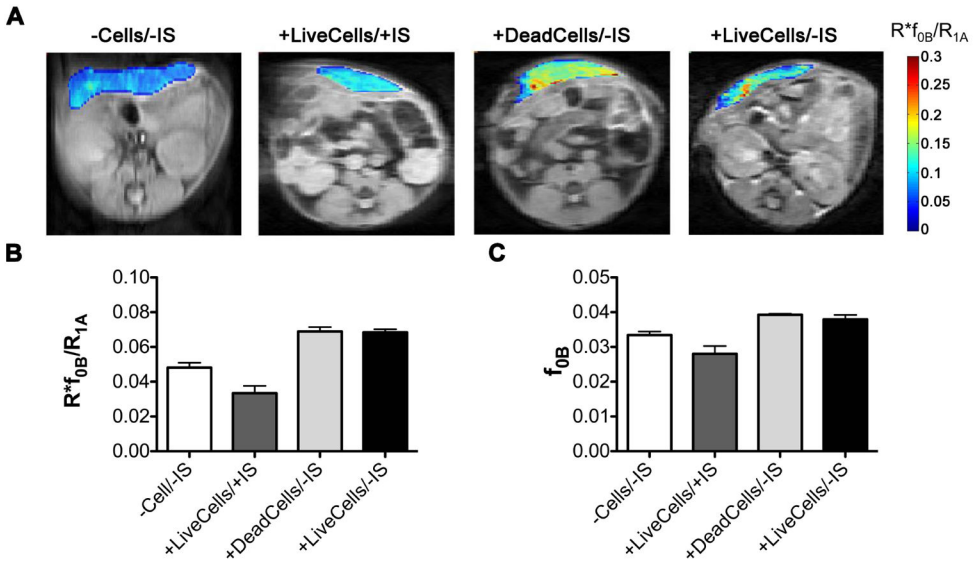

Fig. 6.

(A) Macromolecular ratio maps at −12.5 ppm on Day 1 post-transplantation for the four groups of mice during the acute phase. (B) Calculated macromolecular ratios show that +LiveCells/−IS and +DeadCells/−IS mice had higher ratios compared to +LiveCells/+IS and −Cells/−IS mice, which also had a higher macromolecular fraction (f_{0B}) (C).